

Taming spin susceptibilities in frustrated quantum magnets: Mean-field form and approximate nature of the quantum-to-classical correspondence

Benedikt Schneider^{1,2} and Björn Sbierski³

¹*Department of Physics and Arnold Sommerfeld Center for Theoretical Physics,
Ludwig-Maximilians-Universität München, Theresienstr. 37, 80333 Munich, Germany*

²*Munich Center for Quantum Science and Technology (MCQST), 80799 Munich, Germany*

³*Institut für Theoretische Physik, Universität Tübingen,
Auf der Morgenstelle 14, 72076 Tübingen, Germany*

(Dated: July 15, 2024)

In frustrated quantum magnets the empirically found quantum-to-classical correspondence (QCC) matches the real-space static susceptibility pattern of a quantum spin-1/2 model with its classical counterpart computed at a certain elevated temperature. This puzzling relation was observed via bold line diagrammatic Monte Carlo simulations in dimensions two and three, where the matching was within error bars and seemed valid down to the lowest accessible temperatures T about an order of magnitude smaller than the exchange coupling J . Here we employ resummed spin diagrammatic perturbation theory to show analytically that the QCC breaks at fourth order in J/T and provide the approximate mapping between classical and quantum temperatures. Our treatment further reveals that QCC is an indication of the surprising accuracy with which static correlators can be approximated by a simple renormalized mean-field form. We illustrate this for all models discussed in the context of QCC so far, including a recent example of the $S = 1$ material $\text{K}_2\text{Ni}_2(\text{SO}_4)_3$. The success of the mean-field form is traced back to partial diagrammatic cancellations.

Introduction.—Frustrated quantum magnets remain at the forefront of current research in condensed matter physics [1]. In this arena, enhanced spin fluctuations suppress magnetic ordering and conspire to stabilize delicate highly-entangled quantum states characterized by long-range entanglement and fractional excitations at low temperature T [2, 3]. But how low is “low”? And which experimental observables reveal the sought-after quantum spin liquid properties unambiguously?

While complete answers to these questions, even in theory, remain elusive, impressive progress has been made on the numerical front [4–7]. In 2013, a particularly puzzling empirical observation has been made for the triangular lattice quantum $S = 1/2$ Heisenberg anti-ferromagnet (AFM): In Ref. [8] the bond-resolved spin susceptibility $\chi(\mathbf{r})$ [also referred to as the static spin correlation function, see Eq. (2)] was simulated via bold line diagrammatic Monte Carlo (BDMC). For all temperatures $T \geq 0.375J$ attainable, the intricate and highly featured normalized pattern $\chi(\mathbf{r})/\chi(\mathbf{0})$ (see Fig. 3 left) can be matched by correlation data obtained from the classical ($S = \infty$) vector-spin version of the same Heisenberg model at an empirically obtained elevated temperature $T^{(c)} > T$! This was dubbed the quantum-to-classical correspondence (QCC) [9].

The BDMC [10] is one of the few numerical methods which remains operative for frustrated quantum spin models in high spatial dimensions ($d = 2, 3$) and moderately low $T/J \gtrsim 0.1$. It builds on a complex fermionic representation of spin $S = 1/2$ operators and stochastically samples millions of skeleton Feynman diagrams [11]. Importantly, results for $\chi(\mathbf{r})$ from BDMC are not exact but come with error bars of $\simeq 1\%$. The matching of QCC

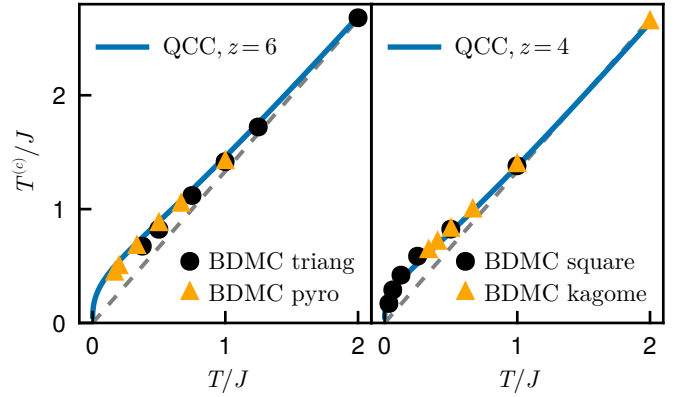


FIG. 1. QCC for systems with a single nearest-neighbor AFM Heisenberg coupling J , left for triangular and pyrochlore lattice with coordination number $z = 6$ and right for kagome and square lattice ($z = 4$). The normalized susceptibility pattern for the quantum $S = 1/2$ system at temperature T was found empirically to be reproduced by the classical (vector-spin) counterpart at $T^{(c)}$ in the BD(MC) studies of Refs. [8, 12, 13] from where the markers are reproduced. The solid lines show the analytical prediction for the *approximate* QCC obtained by numerically inverting Eq. (8), the dashed line denotes the high- T limit $T^{(c)} = 4T/3$.

above is to be understood within these error bars.

In the years following the initial observation, QCC was found wherever the BDMC was aimed at: The square and kagome lattice in $d = 2$ [8, 13], the pyrochlore lattice in $d = 3$ [12] as well as $J_1 - J_2$ models on the square and anisotropic triangular lattices [13]. The corresponding $T^{(c)}(T)$ for various nearest-neighbor quantum models are reproduced from Ref. [8] in Fig. 1 (markers). Re-

cently, QCC was also observed in a $S = 1$ model for the material $\text{K}_2\text{Ni}_2(\text{SO}_4)_3$ consisting of two interconnected $d = 3$ trillium lattices [14], here the quantum data was obtained from the pseudo-fermion functional renormalization group (PFFRG) [7].

As of today, the QCC remains a puzzle with lots of hard-to-ignore anecdotal evidence but no explanation. Why do the celebrated quantum fluctuations maximized for the smallest spin length $S = 1/2$ merely seem to be accounted for classically by an effective heating effect? And would the QCC break down and reveal an approximate nature if a more powerful successor of BDMC could reach lower T ? If not, Ref. [8] speculated, could the empirical $T^{(c)}(T)$ curve be extrapolated to $T = 0$ such that a classical simulation would reveal properties of the highly sought-after quantum ground state?

In this letter we shed analytical light on the origin of QCC building on a recent advance in spin-diagrammatics to be discussed in detail in an upcoming work [15]. The QCC turns out to be only approximate for all finite spin lengths S and dimensions d . We quantify QCC's failure at order $[J/T]^4$, provide a closed-form expression of the (approximate) $T^{(c)}(T)$ curve, and reveal a close connection between QCC and the surprising success of a renormalized mean-field (MF) ansatz for $\chi(\mathbf{r})$. We also quantitatively explain the failure of QCC for the $d = 1$ Heisenberg chain at intermediate temperature, as empirically pointed out already in Ref. [8].

Perturbation theory.—We present a resummed perturbative expansion of the susceptibility in spin- S Heisenberg models. For ease of presentation, we here restrict to nearest-neighbor models on N -site Bravais lattices with single atomic bases (e.g. triangular or square lattices),

$$H = J \sum_{\langle \mathbf{r}, \mathbf{r}' \rangle} \mathbf{S}_{\mathbf{r}} \cdot \mathbf{S}_{\mathbf{r}'}, \quad (1)$$

for generalizations see the supplemental material (SM)[16]. In momentum space, the susceptibility or static spin correlator (at zero Matsubara frequency) is

$$\chi(\mathbf{k}) = \frac{1}{N} \sum_{\mathbf{r}, \mathbf{r}'} e^{-i\mathbf{k} \cdot (\mathbf{r} - \mathbf{r}')} \int_0^\beta d\tau \langle S_{\mathbf{r}}^z(\tau) S_{\mathbf{r}'}^z(0) \rangle, \quad (2)$$

where $\beta = 1/T$ and $S_{\mathbf{r}}^z(\tau)$ is the Heisenberg spin operator at imaginary time τ . The Larkin equation [17, 18] expresses (2) via the set of one- J -irreducible (static) two-legged spin-correlator diagrams $\Sigma(\mathbf{k})$,

$$\chi(\mathbf{k})^{-1} = \Sigma(\mathbf{k})^{-1} + J\gamma(\mathbf{k}), \quad (3)$$

where $\gamma(\mathbf{k}) = \frac{1}{N} \sum_{\langle \mathbf{r}, \mathbf{r}' \rangle} e^{-i\mathbf{k} \cdot (\mathbf{r} - \mathbf{r}')}$ is the spatial Fourier transform of the real-space coupling pattern normalized to unit strength. A diagrammatic representation of Eq. (3) is shown in Fig. 2(a) and a few low-order in J contributions to Σ are depicted in Fig. 2(b).

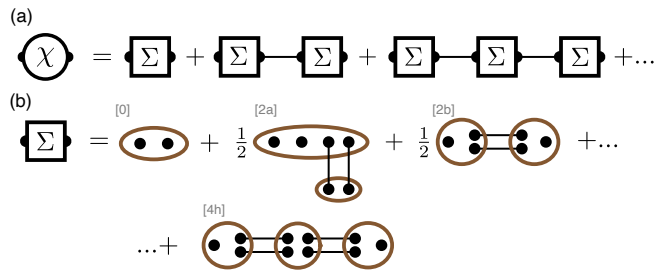


FIG. 2. (a) Diagrammatic representation of the Larkin equation (3). Lines represent the coupling $-J$. (b) Some diagrams contributing to Σ . More details will be presented in [15]. Diagram [4h] and a two-chain $[2b]^2$ contribute to $\Sigma(\mathbf{k})^{-1}$ as $\sim J^4 \gamma(\mathbf{k})^2$.

Replacing the exact Σ in Eq. (3) with its contribution at order J^0 , i.e. with the free-spin (Curie) susceptibility $\Sigma^{(0)} = \beta b_1$ [where $b_1 = S(S+1)/3$] yields the MF approximation [18]. Consequently, terms of higher order capture corrections beyond MF. It is convenient to parameterize the *exact* (inverse) susceptibility $\chi(\mathbf{k})^{-1}$ of Eq. (3) in terms of a renormalized MF part and a correction $\epsilon(\mathbf{k})$ characterized via its beyond-MF momentum dependence,

$$[T\chi(\mathbf{k})]^{-1} = f + g\gamma(\mathbf{k}) + \epsilon(\mathbf{k}). \quad (4)$$

In MF approximation, $f = 1/b_1$, $g = \beta J$ and $\epsilon(\mathbf{k}) = 0$. In that sense, the exact f is the (dimensionless) renormalized on-site inverse susceptibility, while g describes the renormalized coupling. Therefore, we will refer to $\chi(\mathbf{k})$ of the form (4) with $\epsilon(\mathbf{k}) = 0$ as renormalized MF form.

Recent methodological progress to be detailed in [15] provides the expansion of $T\Sigma$ in the dimensionless coupling $X = \beta J$ complete to $O(X^4)$ for various spin models and arbitrary lattice geometry. Focusing on the static correlator for the Heisenberg case, the right-hand side of Eq. (4) is expanded as

$$f = \frac{1}{b_1} + z \left(\frac{1}{6}(6b_1 + 1)X^2 + \frac{1}{24}(4b_1 + 1)X^3 \right) - \frac{I^{(3)}}{6} b_1(6b_1 + 1)X^3 + O(X^4), \quad (5)$$

$$g = X + \frac{X^2}{12} + \frac{X^3}{120} (48b_1^2 + 16b_1 + 3) + O(X^4), \quad (6)$$

$$\epsilon(\mathbf{k}) = -\frac{X^4 b_1}{720} \left[\gamma^2(\mathbf{k}) - z - \frac{I^{(3)}}{z} \gamma(\mathbf{k}) \right] + O(X^5). \quad (7)$$

We defined $I^{(n)} = \int_{\mathbf{k}} \gamma^n(\mathbf{k})$. The special case $I^{(2)} = z$ counts the neighbors per site, the coordination number. For example, the nearest-neighbor Heisenberg model on the d -dimensional hyper-cubic lattice is characterized by $\gamma(\mathbf{k}) = 2 \sum_{l=1}^d \cos k_l$, $z = 2d$ and $I^{(3)} = 0$. The second and third term in brackets of Eq. (7) subtract contributions $\sim \gamma(\mathbf{k})^2$ that can be associated to $O(X^4)$ terms in f and g , respectively.

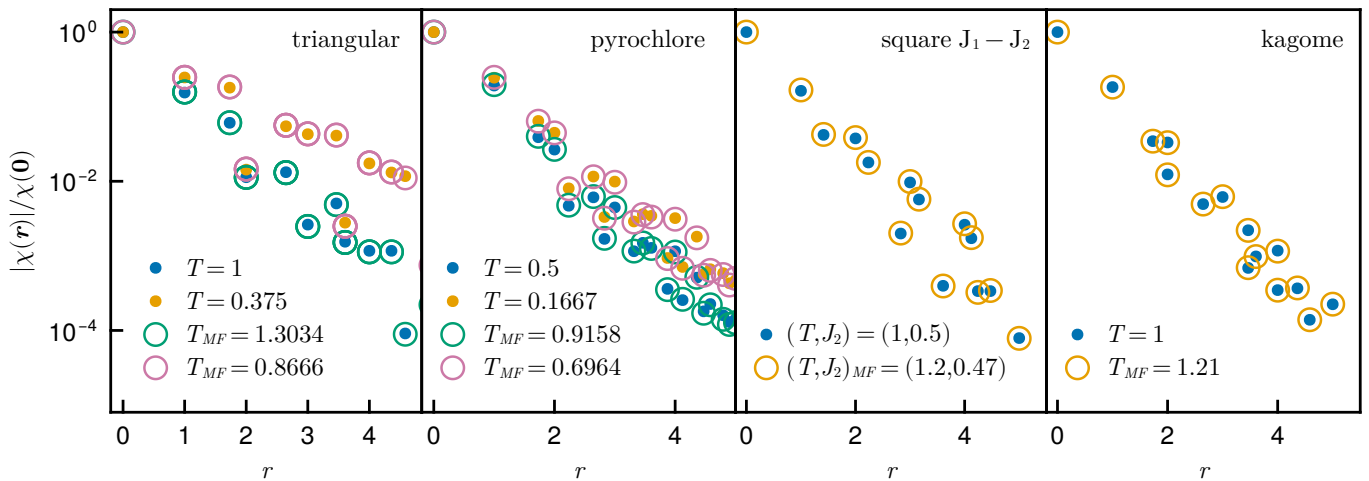


FIG. 3. Absolute values of normalized real space spin susceptibility for AFM $S = 1/2$ Heisenberg models with $J_1 = 1$ and temperature T (dots, data taken from BDMC calculation of Refs. [8, 12, 13]) compared to the renormalized MF form (circles) parameterized with temperature T_{MF} (see text) optimized for best agreement. The almost perfect match for a wide range of models and for rather low T shows the accuracy of the renormalized MF form in $d > 1$ dimensions. For pyrochlore, the mean value of $|\chi(\mathbf{r})|$ with the same r is plotted to match the presentation in Fig. 4 of Ref. [12].

For all the following arguments, it is crucial that corrections to the renormalized MF form in $\epsilon(\mathbf{k})$ appear only from order X^4 on, meaning they are suppressed at high temperatures. Further, the small prefactor in Eq. (7) results from partial diagrammatic cancellation, $\epsilon(\mathbf{k}) \sim (b_1^{-1}[2b]^2 - [4h]) + O(X^5)$, see Fig. 2.

Approximate QCC.—To address the QCC puzzle [8] we consider classical (unit-vector) spins via the $S \rightarrow \infty$ limit. This is straightforward in our general- S formalism after spin-operators in Eqns. (1) and (2) are rescaled by $1/S$. The resulting classical coupling and susceptibility are denoted with superscript (c), hence $\chi^{(c)}(\mathbf{k})^{-1} = \lim_{S \rightarrow \infty} S^2 \chi(\mathbf{k})^{-1}$ with $X \rightarrow X^{(c)}/S^2$. Note that b_1 also depends on S , hence the right-hand sides of Eqns. (5) to (7) simplify by the erasure of quantum effects.

However, as shown above, the susceptibility $\chi(\mathbf{k})$ remains a function of two parameters f, g for all S with $O(X^4)$ corrections. The QCC was discussed for the normalized susceptibility $\chi(\mathbf{k})/\chi(\mathbf{r} = \mathbf{0})$ where $\chi(\mathbf{r} = \mathbf{0}) = \int_{\mathbf{q}} \chi(\mathbf{q})$. The (inverse of the) normalized susceptibility can be computed straightforwardly for both finite S and the classical case. We find an approximate analytic mapping between the two (up to and including order $(X^3) \sim [X^{(c)}]^3$) where f is fixed by the normalization and g can be fixed by relating X to $X^{(c)}$,

$$X = \frac{X^{(c)}}{3b_1} - \frac{(X^{(c)})^2}{108b_1^2} + (X^{(c)})^3 \frac{15b_1z - 12b_1 - 1}{2430b_1^3} + O(X^4). \quad (8)$$

Equivalently, this approximately relates the temperature $T/J = 1/X$ of the quantum spin- S system to that of the classical system, $T^{(c)}/J = 1/X^{(c)}$. In the SM [16] we generalize Eq. (8) to $J_1 - J_2 - \dots$ Heisenberg models with multiple (equivalent) basis sites. For J_1 -models on

lattices with non-trivial basis (e.g. kagome or pyrochlore), Eq. (8) is not changed. This is our first main result.

In Fig. 1, we plot the numerical inverse of Eq. (8) [without $O(X^4)$] for various $S = 1/2$ systems (lines). Note that the lattice only enters via the coordination number z . Results are in good agreement with the empirical data points reproduced from the (BD)MC studies of various $z = 4$ and $z = 6$ models in Refs. [8, 12, 13].

For all lattices considered here, the corresponding classical temperature is always higher than the quantum temperature. Intuitively, quantum fluctuations heat up the system [8]. However, this is not generally the case with the spin-dimer as a counter-example [16].

Renormalized MF form of susceptibility.—The QCC is only approximate and breaks down at order X^4 where first corrections $\epsilon(\mathbf{k})$ to the renormalized MF form appear, see Eq. (7). However, this correction vanishes in the classical limit, $\lim_{S \rightarrow \infty} S^2 \epsilon(\mathbf{k}) = 0 + O((X^{(c)})^6)$. Therefore, from fourth order on, the momentum dependence of the quantum and classical $\chi(\mathbf{k})$ is inherently different, making it fundamentally impossible to extend the mapping $X(X^{(c)})$ in Eq. (8) for the full $\chi(\mathbf{k})$ to order X^4 in an exact way. The QCC is therefore always of approximate nature and, contrary to the speculations in Ref. [8], fails for $T \rightarrow 0$.

However, it turns out that corrections $\epsilon(\mathbf{k})$ to renormalized MF form of $[T\chi(\mathbf{k})]^{-1}$ are relatively small even for small T/J (large X). This can be anticipated from the partial cancellation of diagrams as mentioned above, but it can also be inferred empirically by the high quality of the QCC mapping even for very low T/J , e.g. in the pyrochlore case down to $T/J = 0.1667$ [12]. Formally, the renormalized MF form of $[T\chi(\mathbf{k})]^{-1}$ is a good approximation to the exact value as long as the minimum

of the first two terms $\Delta = f - gz$ (the MF gap) is large compared to $\epsilon(\mathbf{k})$, such that $\|\epsilon\|_1/\Delta \ll 1$. Here we use a L_1 norm in real-space, $\|\epsilon\|_1 = \sum_j |\epsilon_{i,j}|$.

In the following we show that for the $d = 2, 3$ models considered in the context of QCC the susceptibility patterns are very accurately approximated by $\epsilon(\mathbf{k}) \approx 0$ well into the cooperative paramagnetic regime $T/J \gtrsim 0.1$. In Fig. 3 we match the $S = 1/2$ BDMC data from various models treated in Refs. [8, 12, 13] to the renormalized MF form with the empirically optimized MF temperature T_{MF} proportional to the ratio of f and g , $T_{MF} = \frac{fb_1}{g} J$. For the $J_1 - J_2$ models, where the renormalized MF form reads $[T\chi(\mathbf{k})]^{-1} \simeq f + g_1\gamma_1(\mathbf{k}) + g_2\gamma_2(\mathbf{k})$ [16], also J_2 is adjusted, see the labels in Fig. 3. In all instances, the renormalized MF and BDMC data fit very well, even at temperatures below which the analytical mapping based on the truncated version of Eq. (8) would yield reasonable results. This is our second main result. Importantly, this goes beyond the empirical QCC [8] since the exact susceptibilities in the classical case, to which the quantum susceptibilities were matched so far, also feature $O([X^{(c)}]^6)$ corrections to the renormalized MF form, c.f. the discussion above.

As stated by Kulagin et al. [8] the QCC does not hold in the $d = 1$ Heisenberg chain. The susceptibility of this model's classical counterpart is exactly described by the renormalized MF form with $f = \frac{3u^2+3}{1-u^2}$, $g = \frac{3u}{1-u^2}$ and $\epsilon(\mathbf{k}) = 0$ where $u = \coth(X) - 1/X$ [19]: Therefore, QCC can be observed as long as $\|\epsilon(\mathbf{k})\|_1/\Delta \ll 1$ for the quantum correlator. We calculate the susceptibility for the $S = 1/2$ AFM Heisenberg chain with quantum MC [20]. In Fig. 4 we show that $|\Delta|$ vanishes around $T/J \simeq 0.3$ making a renormalized MF approximation of $\chi(k)$ impossible at this temperature. Already for $T/J = 0.5$, the corrections to renormalized MF form are sizable, $\|\epsilon(\mathbf{k})\|_1/\Delta \approx 20\%$. This explains why the range of T/J where QCC could be observed is significantly smaller in $d = 1$ than in the $d = 2, 3$ models, where no violation was found at the temperatures available to BDMC.

Finally, we test the renormalized MF form for a model of a complex realistic material $\text{K}_2\text{Ni}_2(\text{SO}_4)_3$ where QCC was empirically observed by Gonzalez et al. [14]. According to *ab-initio* calculations [14], this $d = 3$ material realizes a $S = 1$ Heisenberg model on two interconnected trillium lattices with $\{J_1, J_2, J_3, J_4, J_5\} = \{0.066, -0.026, 0.144, 1, 0.479\}$ where $J_4 = 1$ is dominant. This model was treated with the ground state PFFRG [7] with results extracted at finite Matsubara frequency cutoff parameter $\Lambda = 0.67J_4$. The latter was argued to act (at least qualitatively) as a finite temperature [21]. Unlike BDMC, the error of PFFRG is uncontrolled. However, empirical confirmation of QCC with $T^{(c)} = 0.35J_4$ [14] suggests that the susceptibility is well described by a renormalized MF form. In Fig. 5 we match the classical MC and PFFRG susceptibilities [14] along multiple

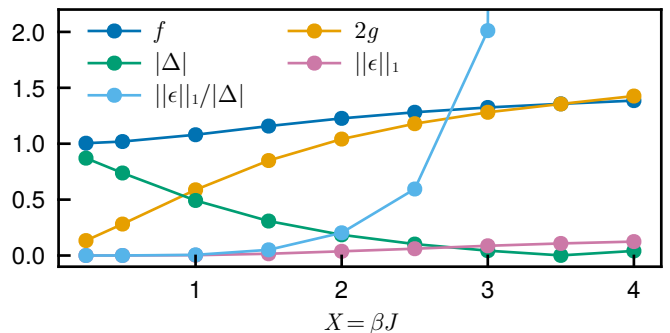


FIG. 4. Parameters of the inverse susceptibility in Eq. (4) for the $S = 1/2$ AFM Heisenberg chain of length $L = 48$. Lines are a guide to the eye. For better visibility f, g, ϵ where all multiplied by the normalization constant: $\chi(r=0) = \int_k \chi(k)$. It can be observed, that the mean field gap Δ closes, rendering a description by the renormalized MF form impossible. The inaccuracy of the renormalized MF form (and thus of QCC) can be seen in the strong increase of $\|\epsilon\|_1/\Delta$.

planes and cuts in \mathbf{k} -space to a renormalized MF form at $T_{MF} = 0.787J_4$ and all J_m unchanged. The quality could be further improved by also renormalizing the latter.

Conclusion.—The approximate description of quantum spin systems with classical theories is a recurring theme [22–25]. However, the so far empirical QCC for the spin susceptibility [8] revisited in this letter stands out by its surprising universality and accuracy even for low temperatures T down to about an order of magnitude below J . Via resummed spin diagrammatic perturbation theory, we showed rigorously that the QCC is only approximate and fails at order $(J/T)^4$. At this order, the spatial dependence of the exact susceptibility deviates from a simple renormalized MF form for $S < \infty$.

In this sense, the QCC can be understood as a symptom of a more fundamental insight put forward in this work: The renormalized MF form almost perfectly accounts for a plethora of spin susceptibility patterns in $d = 2$ and $d = 3$ reported in the literature on the basis of numerically expensive computations. We rationalize this from the partial diagrammatic cancellations of corrections observed at order $(J/T)^4$ but likely also operative at higher orders.

The success of the renormalized MF form is surprising, since ordinary MF theory is only valid for high temperatures or lattices with large coordination numbers. For future work, it is thus an interesting question if the renormalized MF ansatz could inform the development of novel theoretical (renormalization-)methods or experimental data analysis. The latter could be especially relevant for atom-tweezer array quantum simulators where $\chi(\mathbf{r})$ should be directly accessible due to single-site control and measurement capabilities [26]. As a first step, it would be useful to extend the analytical (and approximate) QCC mapping of Eq. (8) to higher orders in (J/T) for better analytical estimation of the renormalized MF

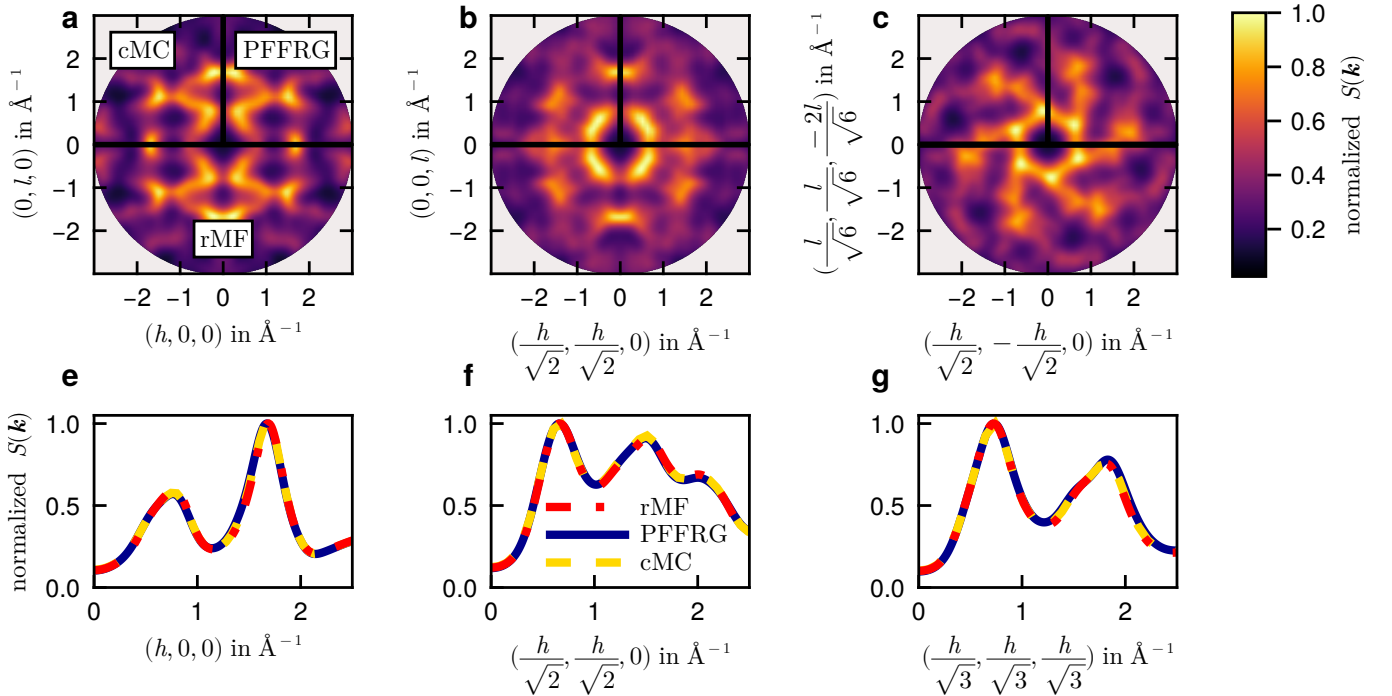


FIG. 5. Static spin structure factor $S(\mathbf{k}) = \sum_{\nu, \nu'} \chi_{\nu, \nu'}(\mathbf{k}) f_{\text{Ni}^{2+}}(\mathbf{k})$ along different planes in reciprocal space, where $f_{\text{Ni}^{2+}}(\mathbf{k})$ is the form factor of the Ni^{2+} ion. Panels (a)-(c) show classical MC results at $T = 0.35J_4$ (top left part of each panel), PFFRG results at flow parameter $\Lambda = 0.58J_4$ (top right), and a fit to the renormalized MF form (rMF, lower half) at $T_{\text{MF}} = 0.787J_4$. Panels (e)-(g) display line cuts along three principal directions. The classical MC and PFFRG data was taken from Ref. [14].

parameters.

Acknowledgment.—We thank Matías G. Gonzalez, Philip Osterholz, Johannes Reuther, Nepomuk Ritz and Manuel Weber for helpful discussions. We acknowledge support from DFG grant no. 524270816. B. Sb. acknowledges support from DFG through the Research Unit FOR 5413/1 (grant no. 465199066). B.Sch. acknowledges funding from the Munich Quantum Valley, supported by the Bavarian state government with funds from the High-tech Agenda Bayern Plus.

-
- [1] C. Lacroix, P. Mendels, and F. Mila, *Introduction to Frustrated Magnetism: Materials, Experiments, Theory*, 2011th ed. (Springer, Berlin Heidelberg, 2011).
- [2] A. Kitaev, Anyons in an exactly solved model and beyond, *Annals of Physics January Special Issue*, **321**, 2 (2006).
- [3] L. Savary and L. Balents, Quantum spin liquids: A review, *Reports on Progress in Physics* **80**, 016502 (2016).
- [4] A. W. Sandvik, A. Avella, and F. Mancini, Computational Studies of Quantum Spin Systems, *AIP Conf. Proc.* **1297**, 135 (2010).
- [5] A. Lohmann, H.-J. Schmidt, and J. Richter, Tenth-order high-temperature expansion for the susceptibility and the specific heat of spin- s Heisenberg models with arbitrary

- exchange patterns: Application to pyrochlore and kagome magnets, *Physical Review B* **89**, 014415 (2014).
- [6] J. Hauschild and F. Pollmann, Efficient numerical simulations with Tensor Networks: Tensor Network Python (TeNPy), *SciPost Physics Lecture Notes*, 005 (2018).
- [7] T. Müller, D. Kiese, N. F. Niggemann, B. Sbierski, J. Reuther, S. Trebst, R. Thomale, and Y. Iqbal, Pseudo-fermion functional renormalization group for spin models, *Reports on Progress in Physics* (2024).
- [8] S. A. Kulagin, N. Prokof'ev, O. A. Starykh, B. Svistunov, and C. N. Varney, Bold Diagrammatic Monte Carlo Method Applied to Fermionized Frustrated Spins, *Physical Review Letters* **110**, 070601 (2013).
- [9] QCC is not to be confused with the fact that quantum phase transitions in d spatial dimensions can share a universality class with a classical counterpart in $d+1$ spatial dimensions [27].
- [10] S. A. Kulagin, N. Prokof'ev, O. A. Starykh, B. Svistunov, and C. N. Varney, Bold diagrammatic Monte Carlo technique for frustrated spin systems, *Physical Review B* **87**, 024407 (2013).
- [11] N. Prokof'ev and B. Svistunov, Bold diagrammatic monte carlo technique: When the sign problem is welcome, *Physical review letters* **99**, 250201 (2007).
- [12] Y. Huang, K. Chen, Y. Deng, N. Prokof'ev, and B. Svistunov, Spin-Ice State of the Quantum Heisenberg Antiferromagnet on the Pyrochlore Lattice, *Physical Review Letters* **116**, 177203 (2016).
- [13] T. Wang, X. Cai, K. Chen, N. V. Prokof'ev, and B. V.

- Svistunov, Quantum-to-classical correspondence in two-dimensional Heisenberg models, *Physical Review B* **101**, 035132 (2020).
- [14] M. G. Gonzalez, V. Nocolak, A. Sharma, V. Favre, J.-R. Soh, A. Magrez, R. Bewley, H. O. Jeschke, J. Reuther, H. M. Rønnow, Y. Iqbal, and I. Živković, *Dynamics of $K_2Ni_2(SO_4)_3$ governed by proximity to a 3D spin liquid model* (2023), [arxiv:2308.11746](https://arxiv.org/abs/2308.11746) [cond-mat].
- [15] B. Schneider *et al.*, manuscript in preparation (2024).
- [16] See the supplemental material for the QCC of the Heisenberg dimer and the generalization to multi-parameter or multi-atomic basis models.
- [17] V. G. Vaks, A. I. Larkin, and S. A. Pikin, Self-consistent field method for the description of phase transitions, *Soviet Physics JETP* **24**, 240 (1967).
- [18] Y. A. Izyumov and Y. N. Skryabin, *Statistical mechanics of magnetically ordered systems* (Consultants Bureau, New York, N.Y, 1988).
- [19] M. E. Fisher, Magnetism in one-dimensional systems-the heisenberg model for infinite spin, *American Journal of Physics* **32**, 343 (1964).
- [20] F. F. Assaad, M. Bercx, F. Goth, A. Götz, J. S. Hofmann, E. Huffman, Z. Liu, F. P. Toldin, J. S. E. Portela, and J. Schwab, The ALF (Algorithms for Lattice Fermions) project release 2.0. Documentation for the auxiliary-field quantum Monte Carlo code, *SciPost Phys. Codebases* , 1 (2022).
- [21] Y. Iqbal, T. Müller, P. Ghosh, M. J. P. Gingras, H. O. Jeschke, S. Rachel, J. Reuther, and R. Thomale, Quantum and Classical Phases of the Pyrochlore Heisenberg Model with Competing Interactions, *Physical Review X* **9**, 011005 (2019).
- [22] S. Chakravarty, B. I. Halperin, and D. R. Nelson, Two-dimensional quantum Heisenberg antiferromagnet at low temperatures, *Physical Review B* **39**, 2344 (1989).
- [23] S. Sachdev, *Quantum Phase Transitions*, 2nd ed. (Cambridge University Press, Cambridge, 2011).
- [24] D. Dahlbom, F. T. Brooks, M. S. Wilson, S. Chi, A. I. Kolesnikov, M. B. Stone, H. Cao, Y.-W. Li, K. Barros, M. Mourigal, C. D. Batista, and X. Bai, Quantum-to-classical crossover in generalized spin systems: Temperature-dependent spin dynamics of FeI_2 , *Physical Review B* **109**, 014427 (2024).
- [25] P. Park, G. Sala, D. M. Pajerowski, A. F. May, J. A. Kolopus, D. Dahlbom, M. B. Stone, G. B. Halász, and A. D. Christianson, Quantum and classical spin dynamics across temperature scales in the $S = 1/2$ Heisenberg antiferromagnet, [arxiv 10.48550/arXiv.2405.08897](https://arxiv.org/abs/2405.08897) (2024), [arXiv:2405.08897](https://arxiv.org/abs/2405.08897) [cond-mat].
- [26] T. Manovitz, S. H. Li, S. Ebadi, R. Samajdar, A. A. Geim, S. J. Evered, D. Bluvstein, H. Zhou, N. U. Köyliüoğlu, J. Feldmeier, P. E. Dolgirev, N. Maskara, M. Kalinowski, S. Sachdev, D. A. Huse, M. Greiner, V. Vuletić, and M. D. Lukin, Quantum coarsening and collective dynamics on a programmable quantum simulator (2024), [arXiv:2407.03249](https://arxiv.org/abs/2407.03249) [cond-mat, physics:physics, physics:quant-ph].
- [27] S. L. Sondhi, S. M. Girvin, J. P. Carini, and D. Shahar, Continuous quantum phase transitions, *Reviews of Modern Physics* **69**, 315 (1997).

SUPPLEMENTAL MATERIAL

GENERALIZATION TO MULTI-PARAMETER MODELS

We consider the QCC mapping for finite-range multi-parameter $J_1 - J_2 - \dots - J_M$ models on general lattices. We restrict the models to the case where all lattice sites are equivalent by symmetry so that $\chi(\mathbf{r} = \mathbf{0})$ used for normalization in the QCC is unambiguous. We start with a spin- S Heisenberg Hamiltonian of the type

$$H = \frac{1}{2} \sum_{\mathbf{r}_\nu, \mathbf{r}'_{\nu'}} J_{(\mathbf{r}_\nu, \mathbf{r}'_{\nu'})} \mathbf{S}_{\mathbf{r}_\nu} \cdot \mathbf{S}_{\mathbf{r}'_{\nu'}} \quad (\text{S1})$$

and on a general Bravais lattice spanned by basis vectors $\{\mathbf{e}_1, \dots, \mathbf{e}_n\}$ with a μ -atomic basis $\{\boldsymbol{\delta}_1, \dots, \boldsymbol{\delta}_\mu\}$, such that each spin position is uniquely described by $\mathbf{r}_\nu = \sum_i r_i \mathbf{e}_i + \boldsymbol{\delta}_\nu$ with $r_i \in \mathbb{Z}$. We define the matrix-valued susceptibility (or static correlator, at vanishing Matsubara frequency)

$$\chi_{\nu\nu'}(\mathbf{k}) = \frac{1}{N} \sum_{\mathbf{r}_\nu, \mathbf{r}'_{\nu'}} e^{-i\mathbf{k} \cdot (\mathbf{r}_\nu - \mathbf{r}'_{\nu'})} \int_0^\beta d\tau \langle S_{\mathbf{r}_\nu}^z(\tau) S_{\mathbf{r}'_{\nu'}}^z(0) \rangle. \quad (\text{S2})$$

Parameterization of the coupling matrix

For each coupling parameter J_1, J_2, \dots, J_M , we define a corresponding unit-strength pattern or coupling matrix

$$\gamma_{m,\nu\nu'}(\mathbf{r}, \mathbf{r}') = \begin{cases} 1 & : J_{\mathbf{r}_\nu, \mathbf{r}'_{\nu'}} = J_m, \\ 0 & : \text{otherwise,} \end{cases} \quad (\text{S3})$$

which takes bonds $(\mathbf{r}_\nu, \mathbf{r}'_{\nu'})$ and outputs unity only if this bond has coupling strength J_m and zero otherwise. With this definition, we obtain with $X_m = \beta J_m$ for $m = 1, 2, \dots, M$,

$$\beta J_{\mathbf{r}_\nu, \mathbf{r}'_{\nu'}} = \sum_{m=1}^M X_m \gamma_{m,\nu\nu'}(\mathbf{r}, \mathbf{r}'). \quad (\text{S4})$$

Fourier transforming the expression gives

$$\beta \mathbf{J}(\mathbf{k}) = \beta \sum_{\mathbf{r}_\nu, \mathbf{r}'_{\nu'}} J_{(\mathbf{r}_\nu, \mathbf{r}'_{\nu'})} e^{-i\mathbf{k} \cdot (\mathbf{r}_\nu - \mathbf{r}'_{\nu'})} = \sum_{m=1}^M X_m \boldsymbol{\gamma}_m(\mathbf{k}) \quad (\text{S5})$$

where we indicated matrices in sublattice space with bold symbols. The $\boldsymbol{\gamma}_m$ are normalized such that $\boldsymbol{\gamma}_m(\mathbf{k}) \delta_{m,n} = \int_{\mathbf{q}} \boldsymbol{\gamma}_m(\mathbf{q}) * \boldsymbol{\gamma}_n(\mathbf{k} - \mathbf{q})$ where $\int_{\mathbf{k}} = \frac{1}{V_{BZ}} \int d\mathbf{k}$ and $*$ is the Hadamard product in sublattice space. Since we assumed that all sites of the lattice are equivalent, the matrices $\boldsymbol{\gamma}_m(\mathbf{k})$ commute $[\boldsymbol{\gamma}_m(\mathbf{k}), \boldsymbol{\gamma}_n(\mathbf{k})] = 0$.

The coordination number z_m with respect to coupling J_m can be expressed via $\int_{\mathbf{k}} \text{Tr}[\boldsymbol{\gamma}_n(\mathbf{k}) \cdot \boldsymbol{\gamma}_m(\mathbf{k})] = \mu z_m \delta_{mn}$ and the number of three-loops made from couplings l, m, n is $\mu I_{l,m,n}^{(3)} = \int_{\mathbf{k}} \text{Tr}[\boldsymbol{\gamma}_l(\mathbf{k}) \cdot \boldsymbol{\gamma}_m(\mathbf{k}) \cdot \boldsymbol{\gamma}_n(\mathbf{k})]$ respectively. Recall that μ is the number of sublattices. These relations follow from the real-space expressions.

Examples for coupling matrices

As an example, the J_1 -Heisenberg model on the kagome lattice is described by $\{\mathbf{e}_1, \mathbf{e}_2\} = \{(2, 0), (1, \sqrt{3})\}$ and $\{\boldsymbol{\delta}_1, \boldsymbol{\delta}_2, \boldsymbol{\delta}_3\} = \{(1, 0), (\frac{1}{2}, \frac{\sqrt{3}}{2}), (-\frac{1}{2}, \frac{\sqrt{3}}{2})\}$ where the triangular Bravais lattice sites are in the center of the hexagons. This lattice yields

$$\boldsymbol{\gamma}(\mathbf{k}) = \begin{pmatrix} 0 & 2 \cos\left(\frac{k_1}{2} + \frac{\sqrt{3}k_2}{2}\right) & 2 \cos\left(\frac{k_1}{2} - \frac{\sqrt{3}k_2}{2}\right) \\ 2 \cos\left(\frac{k_1}{2} + \frac{\sqrt{3}k_2}{2}\right) & 0 & 2 \cos(k_1) \\ 2 \cos\left(\frac{k_1}{2} - \frac{\sqrt{3}k_2}{2}\right) & 2 \cos(k_1) & 0 \end{pmatrix}. \quad (\text{S6})$$

For the anisotropic $J_1 - J_2$ -triangular lattice with horizontal chains coupled by J_1 and interchain coupling J_2 we have $\{\mathbf{e}_1, \mathbf{e}_2\} = \{(1, 0), (1, \sqrt{3})\}$ and $\boldsymbol{\delta}_1 = (0, 0)$ which leads to

$$\gamma_1(\mathbf{k}) = 2 \cos(k_1), \quad (\text{S7})$$

$$\gamma_2(\mathbf{k}) = 2 \cos\left(\frac{k_1}{2} + \frac{\sqrt{3}k_2}{2}\right) + 2 \cos\left(\frac{k_1}{2} - \frac{\sqrt{3}k_2}{2}\right). \quad (\text{S8})$$

Perturbative calculation of χ

The Larkin equation reads in matrix form

$$\boldsymbol{\chi}(\mathbf{k})^{-1} = \boldsymbol{\Sigma}(\mathbf{k})^{-1} + \mathbf{J}(\mathbf{k}). \quad (\text{S9})$$

MF theory amounts to using only the $O([\beta J]^0)$ term, $\boldsymbol{\Sigma}^{(0)}(\mathbf{k}) = b_1 \delta_{\nu', \nu}$ with $b_1 = S(S+1)/3$ the first derivative of the Brillouin function at zero field. Combining Eqns. (S9) and (S5), we parameterize the *exact* inverse correlator with

$$[T\boldsymbol{\chi}(\mathbf{k})]^{-1} = f + \sum_m g_m \gamma_m(\mathbf{k}) + \boldsymbol{\epsilon}(\mathbf{k}). \quad (\text{S10})$$

In MF approximation, $f = \frac{1}{b_1}$, $g_m = X_m$ and $\boldsymbol{\epsilon}(\mathbf{k}) = 0$. Analogously to the one parameter case, in the full theory f is the renormalized on-site interaction, while g_m describes the renormalized MF coupling parameters and $\boldsymbol{\epsilon}(\mathbf{k})$ collects all corrections to the MF form of the correlator.

According to Ref. [1], the inverse static correlator of Eq. (S10) can be expanded in X_m as

$$f = \frac{1}{b_1} + \sum_m z_m \left(\frac{1}{6}(6b_1 + 1)X_m^2 + \frac{1}{24}(4b_1 + 1)X_m^3 \right) - \frac{1}{6}b_1(6b_1 + 1) \sum_{l,m,n} X_m X_l X_n I_{l,m,n}^{(3)} + O(X^4), \quad (\text{S11})$$

$$g_m = X_m + \frac{X_m^2}{12} + \frac{1}{120} (48b_1^2 + 16b_1 + 3) X_m^3 + O(X^4), \quad (\text{S12})$$

$$\boldsymbol{\epsilon}(\mathbf{k}) = -\frac{b_1}{720} \sum_{m,n} (X_m)^2 (X_n)^2 \left(\gamma_m(\mathbf{k}) \cdot \gamma_n(\mathbf{k}) - \delta_{m,n} z_n - \sum_l \frac{I_{l,m,n}^{(3)}}{z_l} \gamma_l(\mathbf{k}) \right) + O(X^5). \quad (\text{S13})$$

Analytic calculation of the approximate QCC

Just as in the one-parameter case $\boldsymbol{\chi}(\mathbf{k})^{-1}$ is of renormalized MF form up to third order in X . It is a function of the $M+1$ parameters f, g_1, g_2, \dots, g_M . Therefore, when comparing the inverse correlator $\boldsymbol{\chi}(\mathbf{k})^{-1} \chi(\mathbf{r} = \mathbf{0})$ normalized with the local correlator $\chi(\mathbf{r} = \mathbf{0}) = \frac{1}{\mu} \text{Tr} \int_{\mathbf{q}} \boldsymbol{\chi}(\mathbf{q})$, with its classical counterpart, we can find a mapping between the two. f is fixed by the normalization and g_m can be fixed by relating X_m and $X_m^{(c)}$,

$$X_m = \frac{X_m^{(c)}}{3b_1} - \frac{(X_m^{(c)})^2}{108b_1^2} + \left(X_m^{(c)}\right)^3 \frac{15b_1 z_m - 12b_1 - 1}{2430b_1^3} + \frac{X_m^{(c)}}{162b_1^2} \sum_{n \neq m} z_n \left(X_n^{(c)}\right)^2 + O(X^4). \quad (\text{S14})$$

This generalizes Eq. (8) of the main text. As explained there, the mapping is only approximate and ceases to exist rigorously at fourth order in X . By inverting Eq. (S14) we capture the QCC of the two-parameter $J_1 - J_2$ models studied in [2]. We present the results in Fig. S1 where the the classical temperatures are predicted quite well. Only the $J_2^{(c)}$ couplings of the square lattice $J_1 - J_2$ with ferromagnetic J_1 show a wrong curvature for small quantum temperatures $T/J_1 \lesssim 0.5$. This signals the breakdown of third order perturbation theory.

QCC FOR THE DIMER

For one parameter models, QCC generally depends on the correlator being a function of two parameters. Since the Heisenberg dimer has only two sites and thus just two susceptibilities χ_{11} and χ_{12} , there exists a trivial, exact QCC.

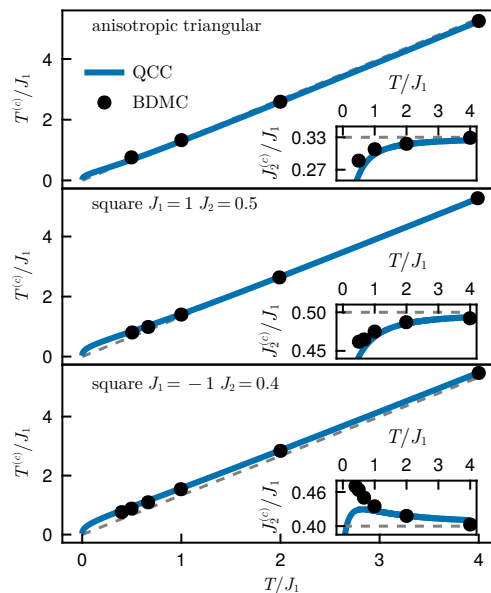


FIG. S1. Mapping between the classical and quantum temperatures for two-parameter models studied by BDMC in Ref. [2]. The solid lines are obtained by inverting Eq. (S14). The markers give the same mapping empirically obtained in Ref. [2]. The dashed line indicates the high temperature asymptotic

The classical correlator is given by

$$T\chi^{(c)}(k) = \frac{1}{3} + \frac{1}{3}(\coth(X^{(c)}) - \frac{1}{X^{(c)}}) \cos(k), \quad (\text{S15})$$

where $k \in \{0, \pi\}$ and the quantum correlator is given as

$$T\chi(k) = \frac{e^X - 1 + X}{2(e^X + 3)} + \frac{e^X - 1 - X}{2(e^X + 3)} \cos(k). \quad (\text{S16})$$

Therefore, the exact QCC between the two is can be found by solving

$$\left(\coth(X^{(c)}) - \frac{1}{X^{(c)}}\right) = \frac{e^X - 1 - X}{e^X - 1 + X} \quad (\text{S17})$$

Setting $J = 1$, for large temperatures $T^{(c)} \simeq \frac{4}{3}T > T$ the system is heated up by the quantum fluctuation but for low temperatures the classical temperature is exponentially reduced $T^{(c)} = \left(\frac{2}{T^2} e^{-1/T}\right) T$. This is related to the fact that the the quantum dimer is gapped so that susceptibilities decrease to zero at low temperature where the state of the classical system can still be easily perturbed. To make up for this difference, $T > T^{(c)}$ at low temperatures.

[1] B. Schneider *et al.*, manuscript in preparation (2024).

[2] T. Wang, X. Cai, K. Chen, N. V. Prokof'ev, and B. V. Svistunov, Quantum-to-classical correspondence in two-dimensional Heisenberg models, *Physical Review B* **101**, 035132 (2020).